

Effect of Lateral Diffusion on Hydrogen Permeation Measurement in Thick Steel Specimens

A. Traidia[†], A. M. El-Sherik, H. Attar, and A. Enezi

Research and Development Center, Saudi Aramco, Saudi Arabia

(Received June 14, 2017; Revised June 14, 2017; Accepted August 18, 2017)

A finite element analysis is proposed to study the effect of specimen dimensions on lateral diffusion of hydrogen during hydrogen permeation flux measurements. The error of measurement on thick specimens because of 1D diffusion approximation may be as much as 70%. A critical condition for accurate measurements is to designate the area of hydrogen monitoring/exit surface smaller than the area of hydrogen charging/entry surface. For thin to medium thickness specimens (ratio of thickness to specimen radius of 5:10 and below), the charging surface should be maximized and the monitoring surface should be minimized. In case of relatively thick specimens (ratio of thickness to specimen radius above of 5:10), use of a hydrogen-diffusion barrier on the specimen boundaries is recommended. It would completely eliminate lateral losses of hydrogen, but cannot eliminate the deviation towards 2D diffusion near the side edges. In such a case, the charging surface should be maximized and the monitoring surface should be as closer in dimension as the charging surface. A regression analysis was carried out and an analytical relationship between the maximum measurement error and the specimen dimensions is proposed.

Keywords: sour corrosion, hydrogen diffusion, HIC, blistering, permeation flux

1. Introduction

Oil and gas transmission pipelines, conventionally made of high strength carbon steels, are quite susceptible to hydrogen embrittlement and the associated forms of degradation, including Hydrogen Induced Cracking (HIC), Step-Wise Cracking (SWC) and Stress-Oriented Hydrogen Induced Cracking (SOHIC) [1]. The mere presence of a very small amount (few wtppm) of wet hydrogen sulphide in the transported hydrocarbons triggers a sour corrosion reaction at inner wall of the pipe. This produces atomic hydrogen that diffuses in the steel lattice and may cause irreversible damage. It has now been well established that the initiation of HIC in pipeline steels takes place at inclusions and second-phase particle-matrix interface [2-8]. In the case non HIC resistant pipelines steels (manufactured prior 1985), the hot rolling manufacturing process led to form elongated Manganese sulphide inclusions (MnS) parallel to the pipe wall and randomly distributed through the steel microstructure with higher density at the steel centre segregation zone [6]. These steels, which are still used in many transmission lines across the world, are of high concern for the pipeline operations and are often re-

ported to suffer from severe HIC and/or SWC [9].

Among others, a key factor in the fitness-for-service assessment of these lines is the accurate knowledge of the hydrogen diffusion flux through the pipe wall as function of the environment conditions, such as pH, H₂S partial pressure and temperature [10]. Due to the non-uniform distribution of non-metallic inclusions along the pipe wall, the use of thin steel membranes, to measure the hydrogen diffusion flux, would not represent actual field conditions where HIC is a bulk phenomenon. The use of thick permeation specimens, manufactured from steel having the same microstructure and thermo-mechanical treatment as the original pipeline, is the most reliable way to accurately measure the hydrogen diffusion flux in field conditions. However, since such specimens are relatively thick (wall thickness up to 30 mm) and due to the finite size of the permeation specimen (in contrast with pipeline configuration), lateral diffusion of hydrogen towards the specimen boundaries can take place inducing a deviation towards 2D diffusion. In such a case, the total amount of hydrogen that enters the steel at the charging side may not be totally measured at the exit/monitoring side. Such a scenario would lead to underestimating the actual hydrogen diffusion flux as compared to that of an actual pipeline configuration, as shown in Fig. 1. Therefore, a careful

[†] Corresponding author: abderrazak.traidia@aramco.com

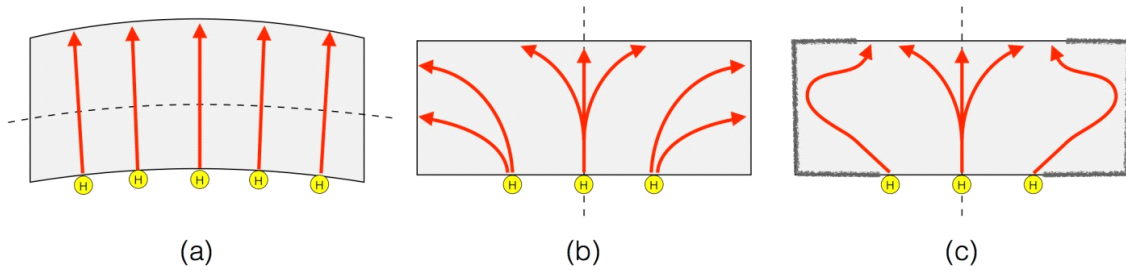


Fig. 1 Comparison of hydrogen diffusion paths through (a) an actual pipeline wall (1D diffusion), (b) a thick steel test plate without a hydrogen diffusion barrier on the sides (2D diffusion and lateral loss of hydrogen), and (c) a test thick steel test plate with hydrogen diffusion barrier on the sides (2D diffusion without lateral loss of hydrogen).

attention should be paid to the design and dimensions of the permeation specimen in order to minimize lateral fluxes of hydrogen and the deviation towards 2D diffusion. The literature review reveals that a recently revised international standard ISO 17081/ASTM G148 [12], developed on the basis of the numerical work by Hutching et al. [12], gives some recommendations regarding the dimensions of the hydrogen permeation specimen. For the measurements to be valid, the standard recommends (1) a minimum ratio of radius of hydrogen charging surface to specimen thickness of 10:1 (independently of other specimen dimensions), or (2) a minimum ratio of 5:1 if the monitoring side of the specimen is reduced to 90% of the area of the charging side. Alternatively, the standard doesn't propose any further solutions for specimen dimensions that may not satisfy the previously mentioned constraints. In addition, for given specimen dimensions that do not satisfy the standard requirements, there is no estimation of the error associated with the deviation from uni-dimensional diffusion towards two-dimensional diffusion induced by the lateral hydrogen fluxes.

In the present work, we have developed a parametric finite element analysis to study the influence of the specimen dimensions (charging surface radius, monitoring/exit surface radius, specimen diameter and thickness) on the magnitude of the lateral hydrogen diffusion fluxes and therefore on the deviation towards a two-dimensional hydrogen diffusion behaviour. Two configurations have been considered; raw permeation specimens (Fig. 1b) and specimens with hydrogen-diffusion barrier introduced on the lateral specimen boundaries, such as a thick oxide layer formed onto the plate's side edges (Fig. 1c). Recommendations have been issued for each configuration and compared with the international standard recommendations.

2. Finite Element Analysis

2.1 Mathematical model

The geometry of the hydrogen permeation specimens used in this study is shown in Fig. 2. The hydrogen charging area (entry surface) is circular with radius, r_{in} and the monitoring area (exit surface) is circular with radius, r_{out} . The specimen thickness is noted as h and the total specimen radius noted as r_t .

Two different configurations are studied as illustrated

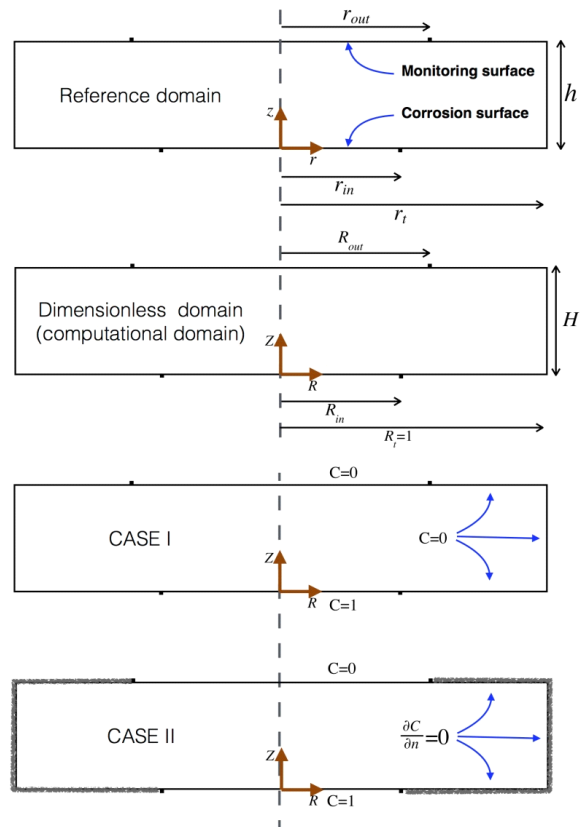


Fig. 2 Schematic representation of the configurations to be simulated and the associated boundary conditions. (Case I: no hydrogen diffusion barrier. Case II: with hydrogen diffusion barrier on the plate sides).

in Fig. 2. The first configuration, case I, corresponds to the usual case where the plate side edges are free of any barrier to hydrogen diffusion (Fig. 1b and Fig. 2c), leading to part of the diffusible hydrogen to escape through these side edges. In this case, only part of the diffusible hydrogen is collected and measured at the exit surface. The second configuration (Fig. 1c and Fig. 2d), case II, corresponds to the case where a hydrogen diffusion oxide barrier is formed on the plate sides to prevent lateral hydrogen losses. In this case, all diffusible hydrogen atoms produced at the entry surface are collected and measured at the exit monitoring surface.

2.2 Mathematical model

The hydrogen diffusion through the steel plates is assumed to follow Fick’s first and second laws as follows [13]:

$$\frac{\partial c}{\partial t} = \nabla \cdot (-D \nabla c) \tag{1}$$

where *c* is the local hydrogen concentration, *D* is hydrogen diffusion coefficient and $\nabla \cdot$ and ∇ respectively denote the divergence and gradient operators.

Due to plate’s symmetry (axi-symmetric conditions) and considering a steady-state analysis, equation 1 becomes:

$$D \frac{\partial^2 c}{\partial r^2} + \frac{D}{r} \frac{\partial c}{\partial r} + D \frac{\partial^2 c}{\partial z^2} = 0 \tag{2}$$

Depending on the simulated configuration (case I or case II, as illustrated in Fig. 2), the resolution of equation 2 is subjected to the following boundary conditions, also reported in Fig. 2:

$$\begin{aligned} \text{Case I: } & \begin{cases} \text{if } (z = 0 \ \& \ r \leq r_{in}): c = c_0; \\ \text{if } (z = h \ \& \ r \leq r_{out}): c = 0; \\ \text{else: } c = 0 \end{cases} \\ \text{Case II: } & \begin{cases} \text{if } (z = 0 \ \& \ r \leq r_{in}): c = c_0; \\ \text{if } (z = h \ \& \ r \leq r_{out}): c = 0; \\ \text{else: } \partial c / \partial n = 0 \end{cases} \end{aligned} \tag{3}$$

Where case I and case II, respectively, denote the absence and presence of hydrogen diffusion barrier on the plate edges.

For ease of mathematical resolution and interpretation of results, it is convenient to convert equation 2 and the corresponding boundary conditions into a dimensionless form. Using the total plate radius and hydrogen charging concentration as reference quantities, the following dimensionless form is derived:

$$\frac{\partial^2 C}{\partial R^2} + \frac{1}{R} \frac{\partial C}{\partial R} + \frac{\partial^2 C}{\partial Z^2} = 0 \tag{4}$$

$$\begin{aligned} \text{Case I: } & \begin{cases} \text{if } (Z = 0 \ \& \ R \leq R_{in}): C = 1; \\ \text{if } (Z = H \ \& \ R \leq R_{out}): C = 0; \\ \text{else: } C = 0 \end{cases} \\ \text{Case II: } & \begin{cases} \text{if } (Z = 0 \ \& \ R \leq R_{in}): C = 1; \\ \text{if } (Z = H \ \& \ R \leq R_{out}): C = 0; \\ \text{else: } \partial C / \partial n = 0 \end{cases} \end{aligned} \tag{5}$$

where *R*, *R_{in}*, *R_{out}*, *Z*, *H* and *C* are dimensionless quantities defined as:

$$R = \frac{r}{r_t}, Z = \frac{z}{r_t}, R_{in} = \frac{r_{in}}{r_t}, R_{out} = \frac{r_{out}}{r_t}, H = \frac{h}{r_t} \text{ and } C = \frac{c}{c_0}$$

The benefit of the above dimensionless form is that the model is now described by three parameters only; *R_{in}*, *R_{out}* and *H*, which represent the ratios of the specimen dimensions to the total specimen radius.

The model equations (equation 4 and 5) have been discretized and solved using the standard finite element method.

2.3 Parametric analysis

A parametric resolution has been carried out to investigate the influence of the specimen dimensions on the results. The variation range of each dimensionless parameter is specified in Table 1.

The analysis of the results will focus on comparing the average flux at the exit surface computed from the 2D model J^{2D} (which would correspond to the hydrogen flux measured in laboratory experiments) with the flux derived

Table 1 Variation ranges of the model parameters used for the parametric simulation

Parameter	Lower limit	Upper limit
<i>R_{in}</i>	0.5 (i.e., 50% of the specimen radius)	1 (i.e., 100% of the specimen radius)
<i>R_{out}</i>	0.5	1
<i>H</i>	0.01	1

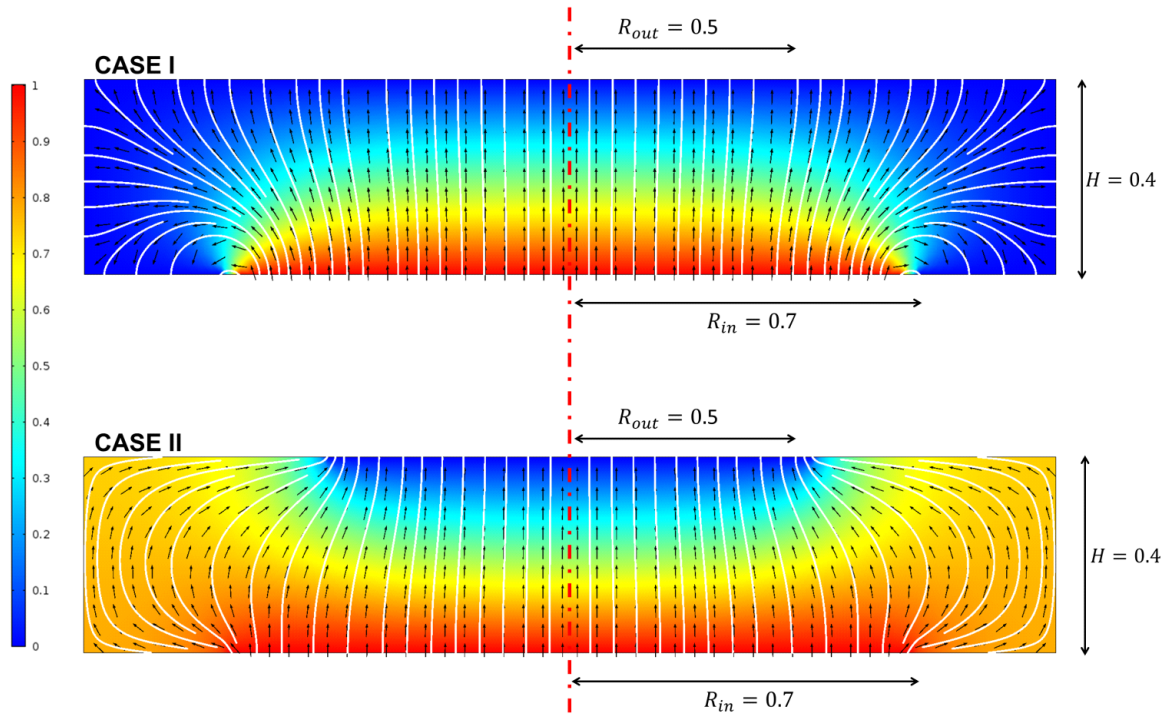


Fig. 3 Comparison between Case I (top) and Case II (bottom) results of the steady state distribution of normalized hydrogen concentration across a specimen with the following dimensions: $H=0.4$, $R_{in}=0.7$ and $R_{out}=0.5$. The vector field of normalized hydrogen diffusion flux and the associated streamlines are also presented.

from the 1D diffusion, noted J^{1D} (which would represent the actual hydrogen permeation flux during the uniform corrosion of a pipeline). The latter being (c_0/h) in a dimensional system, becomes simply $1/H$ in the dimensionless form.

An error indicator, denoted E^{2D-1D} is introduced to quantify the deviation of the 2D computed flux from the common 1D solution, as follows:

$$E^{2D-1D} = \frac{J^{2D} - J^{1D}}{J^{1D}} = \frac{\int_0^{R_{in}} (-\partial C / \partial Z) dR - (1/H)}{(1/H)} \quad (6)$$

3. Results and Discussion

Fig. 3 below shows the distribution of normalized hydrogen concentration through the specimen thickness, as well as the normalized vector field of hydrogen flux and the associated streamlines on a typical geometry. The results for both studied configurations are presented. As expected, case I exhibits typical deviation from 1D towards 2D diffusion. Due to the low chemical potential on the open specimen boundaries, hydrogen diffuses towards the edges, then recombines into molecular hydrogen and es-

capas into the atmosphere. Only part of the diffused hydrogen is measured at the monitoring surface, where hydrogen diffusion is still fairly uni-dimensional. In this case (I) the hydrogen flux measurements in the laboratory would underestimate the actual 1D diffusion flux in field conditions. In contrast, the presence of a hydrogen-diffusion barrier on the specimen' side boundaries (case II) prevents hydrogen to escape and diverts all diffused hydrogen towards the monitoring surface at the exit. Since E^{2D-1D} measures the deviation from 1D towards 2D diffusion, it clearly appears that the deviation induced by the diverted flux at the specimen boundaries in case II would be more pronounced for thick specimens. A careful attention should therefore be paid to the choice of the specimen dimensions, since in this case, since the hydrogen flux measured at the exit surface may overestimate the actual 1D diffusion flux in field conditions. This is discussed in further details in the following of this paper.

3.1 Charging surface larger than monitoring surface

Fig. 4 shows the evolution of the computed error E^{2D-1D} as function of the normalized specimen thickness for different values of normalized inner and outer radii, and for the two studied configurations; case I (raw specimens) and case II (specimens with hydrogen diffusion barrier

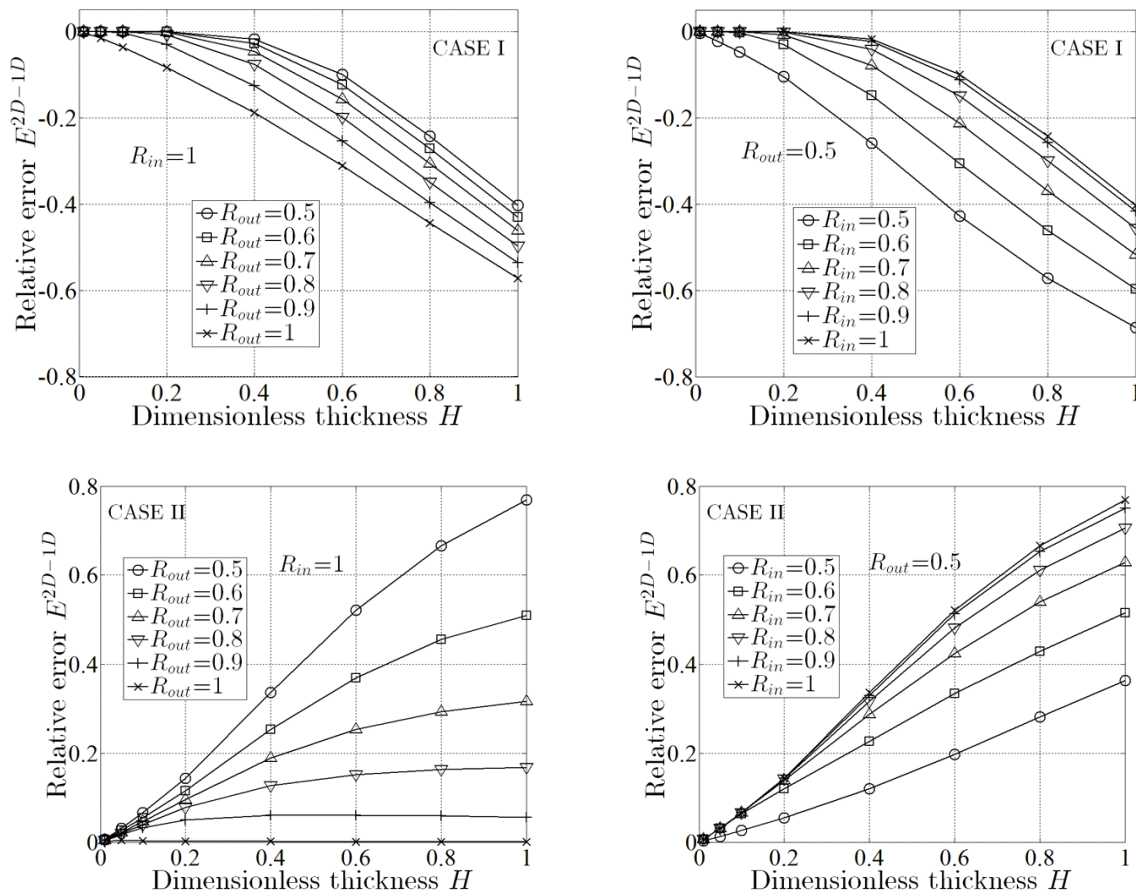


Fig. 4 Deviation error towards 2D diffusion (E^{2D-1D}) as function of the normalized specimen thickness H for specimens with hydrogen charging surface larger than the monitoring/exit surface. Results for raw specimens (top) and specimens with hydrogen-diffusion barrier (bottom) are presented.

on the outside boundaries). All cases presented in Fig. 4 satisfy the critical condition, $R_{in} \geq R_{out}$, i.e., the hydrogen charging/entry surface is larger than or equal to the monitoring/exit surface.

For the raw specimens (case I), as expected, the error is negative and increases, in absolute value, with increasing specimen thickness, which is naturally due to the deviation from the ideal 1D diffusion behaviour. This means that hydrogen flux measured in lab experiments J^{2D} (which corresponds to the 2D model) may significantly underestimate the actual hydrogen flux in field conditions J^{1D} (1D diffusion), since the error associated with lateral diffusion fluxes and loss of hydrogen through the specimen boundaries are found to be critically important. The maximum computed error is about 70%, which takes place for the worst case: small corrosion area ($R_{in} = 0.5$), small monitoring area ($R_{out} = 0.5$) and thick specimen ($H = 1$). At fixed specimen radius, the error increases with decreas-

ing charging surface and increasing monitoring surface. Therefore, the area of the hydrogen entry surface must be maximized, and the area of the monitoring surface minimized in order to minimize the error associated with lateral diffusions fluxes. This result was highlighted in the previous work by Hutching *et al.* [12] and is in very good agreement with ISO 17081 recommendations [11].

For relatively thick specimens, lateral losses may become quite significant and therefore the use of a hydrogen-diffusion barrier on the specimen boundaries may appear to be a useful solution. When a hydrogen diffusion barrier is introduced on the specimen boundaries, Fig. 4 shows that the error associated with lateral hydrogen diffusion may become worst if a careful attention is not paid to the choice of specimen dimensions. Indeed, by introducing a hydrogen-diffusion barrier on the specimen boundaries, the losses of hydrogen by lateral diffusion are completely eliminated, however, the deviations towards

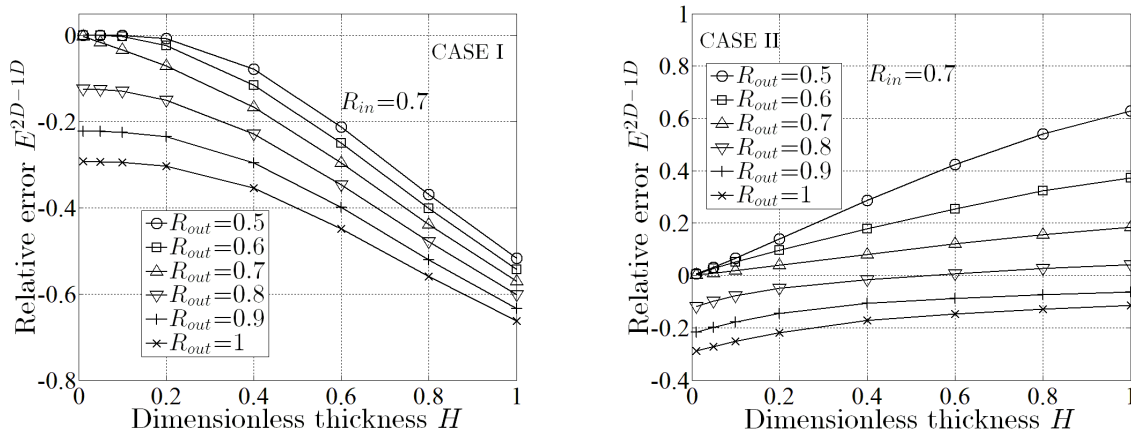


Fig. 5 Deviation error towards 2D diffusion (E^{2D-1D}) as function of the normalized specimen thickness H for specimens with hydrogen charging surface smaller than the monitoring/exit surface. Results for raw specimens (left) and specimens with hydrogen-diffusion barrier (right) are presented.

Table 2 Multiple Linear Regression analysis results on FEM results with $R_{in} \geq R_{out}$

Coefficient	Case I (raw specimens)		Case II (with hydrogen-diffusion barrier)	
	Estimated value	Standard deviation	Estimated value	Standard deviation
α_0	-0.43	0.06	0	0
α_1	1.11	0.13	1.26	0.14
α_2	0	0	-1.23	0.14
α_3	-0.39	0.03	1.10	0.03
α_{12}	0.47	0.17	0.44	0.18
α_{13}	0.61	0.04	0.75	0.04
α_{23}	-0.39	0.04	-1.83	0.04
α_{11}	-0.84	0.1	-0.95	0.11
α_{22}	-0.37	0.1	0.60	0.10
α_{33}	-0.39	0.02	-0.14	0.02
	RMSE	0.021	RMSE	0.023
	R-squared	0.989	R-squared	0.985

2D diffusion near the specimen boundaries are still present (as illustrated by the streamlines in Fig. 3), resulting in positive error values. As a consequence, the hydrogen flux measured in the laboratory experiments, J^{2D} , may overestimate the actual hydrogen flux in field conditions, J^{1D} , except for the optimum case $R_{in} = R_{out} = 1$ (where the error is zero and is independent of the specimen thickness). From the results presented in Fig. 4, it appears that for relatively thick specimen (ratio of thickness to specimen radius above of 5:10), a hydrogen-diffusion barrier should be used but with a maximum hydrogen charging surface and a monitoring surface as closer in dimension as the charging surface.

3.2 Charging surface smaller than monitoring surface

Fig. 5 illustrates the evolution of the error, for both studied configurations, in case where the hydrogen charging surface may become smaller than the hydrogen mon-

itoring surface. This figure shows that the error drastically increases for the cases where $R_{in} < R_{out}$. This fact is not related to the lateral diffusion of hydrogen, but rather to simple geometrical considerations. Actually, when $R_{in} < R_{out}$, the material acts like an inverted cone flow, where the velocity is smaller at the exit compared to that at the entry surface. This leads to a decrease in the measured hydrogen flux at the corrosion surface, which in addition to the lateral losses of hydrogen, results in a drastic increase in the error, even for thin membranes. This important finding clearly shows that the recommendations given in ISO 17081 are valid only when the hydrogen charging surface is larger than the monitoring exit surface. Indeed, for all configurations with ratio of hydrogen charging surface radius to specimen thickness greater than 10:1 (i.e, a-priori respecting ISO 17081 recommendations), but with hydrogen charging surface smaller than the oxidation

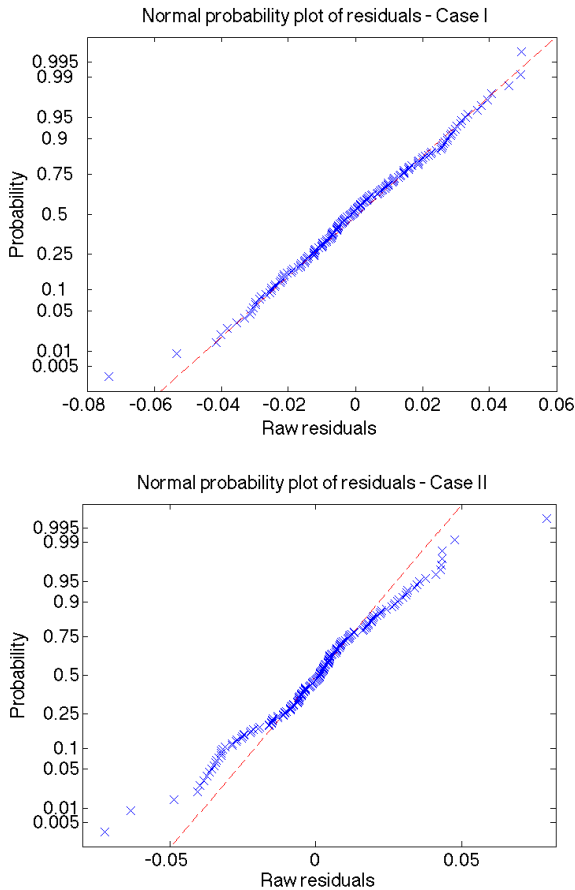


Fig. 6 Normal probability plot of raw residuals for the regression models on Case I (left) and Case II (right) FEM results.

surface, the computed errors are at the highest level. We therefore recommend considering $R_{in} \geq R_{out}$ (critical condition) for all hydrogen permeation tests, no matter what the specimen thickness is.

3.3 Multiple Linear Regression analysis (MLR)

In the present section we carried a Multiple Linear Regression analysis (MLR) on the FEM results obtained for the sets of data where the critical condition is satisfied ($R_{in} \geq R_{out}$). The purpose of this analysis is to propose an analytical relationship between the error E^{2D-1D} and the permeation specimen dimensions, for both cases (I and II). This analytical relationship could be further used to anticipate and predict the error that might be introduced when using a permeation specimen with relatively high thickness.

After testing different regression functions, the quadratic regression was found to give the best fit to the FEM results. The regression function for both case I and case II takes the form presented in equation 7. The results of

the MLR analysis are summarized table 2.

$$E^{2D-1D} = \alpha_0 + \alpha_1 R_{in} + \alpha_2 R_{out} + \alpha_3 H + \alpha_{12} R_{in} R_{out} + \alpha_{13} R_{in} H + \alpha_{23} R_{out} H + \alpha_{11} R_{in}^2 + \alpha_{22} R_{out}^2 + \alpha_{33} H^2 \quad (7)$$

The fitted models have excellent R-squared values, illustrating that the fitted models capture almost 99% of the variability in the FEM data. Fig. 6 shows the residual probability plots for the two regression models. The maximum value of raw residuals is about 5%.

4. Conclusions

The present work discussed the results of a finite element model used to simulate the influence of lateral diffusion of hydrogen on the accuracy of permeation rate measurements in steel specimens. The computed results showed that the accuracy of laboratory measurements could be greatly reduced for experiments carried out on relatively thick specimens. This was attributed to the lateral loss of hydrogen through the specimen boundaries, which induces a deviation from 1D towards 2D diffusion of hydrogen. The use of a hydrogen-diffusion barrier on the specimen boundaries would eliminate hydrogen losses, but cannot eliminate the deviation towards 2D diffusion near the side edges. Therefore a careful attention should be paid to the choice of corrosion and monitoring surface dimensions in order not to overestimate the hydrogen permeation flux as compared to field conditions.

Parametric FEM simulations were carried out and showed that a critical condition is to always have the entry surface larger in dimension than the exit surface. In addition, for relatively thin to medium thickness coupons (ratio of thickness to specimen radius of 5:10 and below), the corrosion surface should be maximized and the monitoring surface minimized, without any modification to the specimen boundary conditions. In contrast, for thick specimens (ratio of thickness to specimen radius of 5:10 and above), the use of hydrogen diffusion barrier on the specimen boundaries is recommended. An additional requirement is maximizing the hydrogen charging surface and having a monitoring surface as closer in dimension as the charging surface. A regression analysis was conducted on the FEM results and showed that the error associate with lateral diffusion can be fairly correlated with the specimen dimensions using a quadratic regression function.

Acknowledgments

The authors are grateful to the Research and Development

Centre of Saudi Aramco for the authorization and support to publish the present work.

References

1. International Standard NACE MR0175 / ISO 15156-2, Petroleum and natural gas industries — Materials for use in H₂S-containing environments in oil and gas production. Part 2: Cracking-resistant carbon and low alloy steels, and the use of cast irons (2003).
2. T. Hara, H. Asahi, and H. Ogawa, *Corrosion*, **60**, 1113 (2004).
3. M. Iino, *Metall. Trans., A*, **9**, 1581 (1978).
4. C. P. Ju and J. M. Rigsbee, *Mater. Sci. Eng.*, **74**, 47 (1985).
5. M. Y. B. Zakaria and T. J. Davies, *J. Mater. Sci.*, **28**, 3322 (1993).
6. G. Domizzi, G. Anteri, and J. Ovejero-Garcia, *Corros. Sci.*, **43**, 325 (2001).
7. M. Elboudjaini, R. W. Revie, and C. DeRushie, *Proc. Corrosion 2003 Conf.*, paper 03528, NACE International, San Diego, California (2003).
8. M. Elboudjaini, M. T. Shehata, V. S. Sastri, R. W. Revie, and R. R. Ramsingh, *Proc. Corrosion 98 Conf.*, paper 748, NACE International, NACE International, San Diego, California (1998).
9. M. A. Abufour, and Y. A. El-Said, *Proc. 5th Middle East NDT Conf.*, pp. 1-6, Jubail Industrial College, Bahrain (2009).
10. A. Traidia, M. Alfano, L. Lubineau, S. Duval, and A. Sherik, *Int. J. Hydrogen Energ.*, **37**, 12214 (2012).
11. International Standard ISO 17081 / ASTM G148, Method of measurement of hydrogen permeation and determination of hydrogen uptake and transport in metals by an electrochemical technique (2014).
12. R. B. Hutchings, D. H. Ferris, and A. Turnbull, *Brit. Corros. J.*, **28**, 309 (1993).
13. J. Crank, *The Mathematics of Diffusion*, 2nd ed., pp. 1-414, Clarendon Press, Oxford, New York (1975).